Applied Catalysis B: Environmental 168-169 (2015) 524–530

Contents lists available at ScienceDirect

Applied Catalysis B: Environmental

journal homepage: www.elsevier.com/locate/apcatb

Hydrogen production from propane steam reforming over $Ir/Ce_{0.75}Zr_{0.25}O_2$ catalyst

Tengfei Hou [a], Bo Yu [b], Shaoyin Zhang [a], Jianghua Zhang [a], Dazhi Wang [a], Tongkuan Xu [a], Li Cui [a], Weijie Cai [a,*]

[a] Faculty of Light Industry and Chemical Engineering, Dalian Polytechnic University, 116023 Dalian, China
[b] College of Materials Science and Engineering, Dalian Jiaotong University, 116023 Dalian, China

ARTICLE INFO

Article history:
Received 12 November 2014
Received in revised form 15 January 2015
Accepted 19 January 2015
Available online 20 January 2015

Keywords:
$Ir/Ce_{0.75}Zr_{0.25}O_2$
Hydrogen
Propane
Steam reforming

ABSTRACT

Steam reforming of propane over a novel $Ir/Ce_{0.75}Zr_{0.25}O_2$ catalyst was investigated. Various techniques such as X-ray diffraction (XRD), temperature-programmed reduction (TPR), high resolution transmission electron microscopy (HRTEM), and oxygen storage capacity (OSC) etc were used to characterize the as-prepared catalysts in order to elucidate the catalyst structure-performance relationship. The doping of ZrO_2 into the CeO_2 lattice greatly improved the redox property of the CeO_2 by creating more surface oxygen vacancies. Stability test revealed that the $Ir/Ce_{0.75}Zr_{0.25}O_2$ sample exhibited rather stable catalytic behavior for 65 h time-on-stream without obvious deactivation, which was assigned to the efficient prevention of the sintering of the highly dispersed Ir particles through the strong interaction between Ir and CeO_2 support and to the significant resistance to coke deposition due to the excellent OSC of $Ce_{0.75}Zr_{0.25}O_2$ support.

© 2015 Elsevier B.V. All rights reserved.

1. Introduction

With increasing concerns about the depletion of fossil fuels and environmental pollution, hydrogen has been regarded as the most promising energy carrier in transportation and domestic applications [1–3]. Nowadays, hydrogen is mainly produced by hydrocarbons and/or alcohols reforming. Among various hydrocarbon feed stocks, liquefied petroleum gas (LPG) appears as the attractive feedstock for hydrogen and/or syngas formation, due to their existing distribution and supply infrastructure [4–6]. Hydrogen and syngas are the basic raw materials to produce synthetic liquid fuels (SLFS) and chemicals via the industrially available processes [7,8]. LPG is a mixture of petroleum gases that exists in a liquid state at ambient temperatures under moderate pressures (less than 1.5 MPa). It is inexpensive and mainly consists of propane in many countries such as U.S./Canadian LPG [9,10]. Hence, propane has also been accepted as a practical feedstock for hydrogen production due to its abundance and its well-established infrastructure in modern cities.

Up to date, steam reforming (SR), partial oxidation (POX), oxidative steam reforming (OSR) and dry reforming (CO_2 reforming) are the major routes for hydrogen and/or syngas production from propane [11–14]. Most studies have focused on the steam reforming of propane using supported Ni, Co, Ru and Pd catalysts operated at relatively high temperatures, typically 500–700 °C [15–17]. Among these catalysts, noble metals are the more efficient system compared to the transition metals with respect to propane conversion and hydrogen selectivity, probably due to their strong capacity for breaking the C—C bond of propane. Zapf et al. [10] applied Rh nanoparticles as precursors to prepare Rh/Al_2O_3 catalysts for propane steam reforming. No obvious deactivation was observed during 140 h long-term test. In the recent studies of Shen group [18–21], a novel Ir/CeO_2 system has been developed for ethanol reforming, which exhibited excellent activity/stability at relatively low temperatures even under the stoichiometric feed conditions. It has frequently been shown that support also plays a critical role in the activity/selectivity and stability of the catalyst for hydrocarbon or alcohol reforming [22–25]. In this respect, the excellent performances of CeO_2-supported catalysts known as the high catalytic activity and resistance against carbon deposition, have been tentatively related to the high OSC of CeO_2 and to the strong interaction between CeO_2 and the supported active metal [26]. Insertion of Zr^{4+} into the CeO_2 lattice structure might result in structural

* Corresponding author. Tel.: +86 41186324482; fax: +86 41186322228.
E-mail address: caiwj@dlpu.edu.cn (W. Cai).

http://dx.doi.org/10.1016/j.apcatb.2015.01.023
0926-3373/© 2015 Elsevier B.V. All rights reserved.

distortions of the CeO_2 fluorite lattice and improve its OSC, thermal stability and resistance to sintering. Since the ionic radius of Zr^{4+} is smaller than the value of Ce^{4+}, it can contribute to remove the strain associated with the increase of size during the Ce^{4+} to Ce^{3+} transition, and therefore to enhance the CeO_2 redox capacity and facilitate the oxygen mobility [26,27]. Computer simulation studies revealed that even small addition of ZrO_2 greatly promoted bulk Ce^{4+} reduction compared to pure CeO_2 [28]. In fact, the high OSC of cubic $Ce_{0.75}Zr_{0.25}O_2$ can increase the availability of surface oxygen, which is favorable for the WGS reaction increasing the H_2 yield in reformation reactions [29]. As to CeO_2—ZrO_2 supports, the Ce/Zr molar ratio plays an important role in the catalytic behavior in reforming processes. Roh et al. [30] investigated the influence of Ce/Zr ratio for ethanol steam reforming over Rh/CeO_2—ZrO_2 catalyst. $Rh/Ce_{0.8}Zr_{0.2}O_2$ presented the highest H_2 and CO_2 yield and the lowest deactivation rate due to the less formation of carbon deposits. Hence, a study of ethanol steam reforming over $Ni/Ce_{1-x}Zr_xO_2$ (x = 0,0.26, 0.59, 0.84,1) indicated that $Ni/Ce_{0.74}Zr_{0.26}O_2$ sample exhibited the highest activity, which was due to it having the most reduced nickel available for reaction [29].

Taking into account the recent results regarding ethanol reforming together with the background of the application of CeO_2—ZrO_2-supported catalysts in the reforming of bio-butanol raw mixture [26], here we further investigate steam reforming of propane over $Ir/Ce_{0.75}Zr_{0.25}O_2$ catalyst (Ce/Zr = 3 molar ratio). The reason why we selected this Ce/Zr molar ratio was due to the guidance of the previous literatures [29,30]. Hence, the aim of this work is to elucidate the main parameters that influence the behavior of $Ir/Ce_{0.75}Zr_{0.25}O_2$ sample in propane steam reforming. Catalysts were tested at initial conversion values lower than 100% and this allowed to following the deactivation. In order to establish the possible structure-catalytic performance relationship, catalysts were characterized using: TPR, XRD, X-ray photoelectron spectroscopy (XPS), CO_2 temperature programmed desorption (CO_2–TPD), followed by HRTEM.

2. Experimental

2.1. Catalyst preparation

$Ce_{0.75}Zr_{0.25}O_2$ support (Ce/Zr = 3 molar ratio) was prepared by co-precipitation of ammonia cerium nitrate and zirconium nitrate with urea in aqueous solution. Firstly, the mixture of $(NH_4)_2Ce(NO_3)_6$, $Zr(NO_3)_4{\cdot}5H_2O$ and urea was dissolved into deionied water and then gradually heated to 90 °C under stirring and kept at this temperature for 6 h. After filtration and thorough washing with water, the precipitate was dried overnight at 100 °C and further calcined at 400 °C for 5 h in static air.

$Ir/Ce_{0.75}Zr_{0.25}O_2$ catalyst with an Ir nominal loading of 2 wt.% was synthesized by a deposition–precipitation method. The as-prepared $Ce_{0.75}Zr_{0.25}O_2$ powders were suspended in aqueous solution containing appropriate amounts of Ir precursor ($H_2IrCl_6{\cdot}6H_2O$), and the mixture was heated to 75 °C under continuous stirring. A 0.25 M Na_2CO_3 aqueous solution was gradually added until the pH value of the mixture reached 9.0, followed by further aging at 75 °C for 1 h, during which the precipitate was exclusively deposited onto the CeO_2 surface. After filtration and washing with water, the obtained solid was dried at 100 °C overnight and finally calcined at 400 °C for 5 h in static air.

2.2. Catalyst characterization

The actual metal content in $Ir/Ce_{0.75}Zr_{0.25}O_2$ catalyst was analyzed by an inductively coupled plasma (ICP) atomic emission spectrometer (PLASMA-SPEC-II).

XRD patterns were recorded using a Rigaku D/MAX-RB diffractor with Cu Kα radiation source operating at 40 kV and 100 mA. The mean crystallite sizes of ceria were calculated according to the Scherrer equation [31].

OSC of the as-prepared catalysts was measured using the oxygen pulse injection method. Before analysis, the samples (50 mg) were reduced with H_2/Ar (12 vol.%, 50 mL/min) at 800 °C. Then, they were cooled to 300 °C under Ar flow (50 mL/min). A stream of O_2/He (10 vol.%) was periodically injected into the reduced sample until saturation and accordingly the oxygen consumption was calculated.

HRTEM images were obtained using Philips Tecnai G220 microscope operating at 300 kV. Specimens were prepared by ultrasonically suspending the sample in ethanol. A drop of the suspension was deposited to a thin carbon film supported on a standard copper grid and dried in air.

N_2 adsorption–desorption isotherms were recorded at −196 °C using a Nova 4200e instrument (Quantachrome). Before the measurement, the sample was outgassed at 300 °C for 2 h. The specific surface area was calculated by multipoint BET analysis of the nitrogen adsorption isotherms.

H_2–TPR was preformed with a Micromeritics AutoChem. II chemisorption analyzer. About 40 mg catalyst sample was pretreated at 100 °C for 1 h under flowing He (50 mL/min). After cooling down to room temperature, the sample was exposed to a flow of 12 vol.% H_2/Ar (50 mL/min), and the temperature was increased linearly at 10 °C/min.

XPS was measured on a KRATOS AXIS Ultra DLD spectrometer equipped with a hemispherical electron analyzer and an Al anode (Al Kα = 1486.6 eV) powered at 150 W. The C_{1s} peak at 284.6 eV was used as an internal standard for peak position measurement. The areas of the peaks were estimated by calculating the integrality of each peak after subtracting a Shirley background and fitting the experimental peak to a combination of Lorentzian/Gaussian lines of variable proportions.

CO_2–TPD experiment was carried out using a flow system equipped with a mass spectrometry. Prior to the experiment, the sample was pretreated at 300 °C for 1 h in Ar. Then it was cooled down and CO_2 was adsorbed at 25 °C. After being purged with Ar to remove the weakly adsorbed CO_2, the sample was heated again from 25 °C to 800 °C at a heating rate of 10 °C/min in Ar flow. The signal of desorption CO_2 was monitored online with mass spectrometry (INFICON IPC400).

The formation of the carbonaceous deposits during steady-state catalytic experiments was quantified by TPO of the aged catalyst. 100 mg of the used catalyst was loaded in a microreactor and the system was heated from 25 °C to 700 °C at a rate of 5 °C/min with a flow of 5 vol.% O_2/Ar mixture (100 mL/min). The effluents were analyzed by on-line mass spectrometry (Inficon quadrupole).

2.3. Catalytic measurements

Propane steam reforming was carried out in a fixed-bed quartz reactor under atmospheric pressure. The catalyst (100 mg) (grain size 40–60 mesh) was loaded and sandwiched by two quartz wool layers. Prior to reaction, the catalyst was reduced with 5 vol.% H_2/Ar (100 mL/min) at 400 °C for 1 h. Water was fed by a micro-pump to a vaporizer heated to 200 °C. The flow rate of propane was regulated by a mass flow controller. The effluent from the reactor was analyzed by online gas chromatography. H_2, CO, and CO_2 were separated by a packed column (HayeSep D) and analyzed by a thermal conductivity detector (TCD) using He as carrier gas. Hydrocarbons were separated with a capillary column (INNOWAX) and analyzed with a flame ionization detector (FID). Propane conversion, product concentrations were calculated and listed as follows:

Propane conversion is calculated according to:

$$X_{propane} = \left\{ \left[\sum n*(C_i)_{outlet} \right] - \left[3*(C_{propane})_{outlet} \right] \right\} / \left[\sum n*(C_i)_{outlet} \right] \quad (eq.1)$$

with $(C_i)_{outlet}$: molar concentration of carbon containing species (labeled as i) in the outlet gas.

$n = 1$ for CO, CO_2 and CH_4; $n = 3$ for C_3H_8, C_3H_6

The molar concentration of hydrogen in the outlet dry gas (except water) is calculated according to:

$$C*_{H2} = (C_{H2})_{outlet} / \left[(C_{H2})_{outlet} + \sum (C_i)_{outlet} \right] \quad (eq.2)$$

Molar concentrations of carbon containing species (labeled as i) in the outlet dry gas (except water) are calculated according to:

$$C*_i = (C_i)_{outlet} / \left[(C_{H2})_{outlet} + \sum (C_i)_{outlet} \right] \quad (eq.3)$$

with $(C_{H2})_{outlet}$: molar concentration of hydrogen in the outlet gas.

3. Results and discussion

3.1. Characteristics of the catalyst

ICP analysis revealed that the amount of Ir in the $Ir/Ce_{0.75}Zr_{0.25}O_2$ sample was 1.95 wt.%, as targeted. BET surface area of the catalyst was measured to be 160 m^2/g. Fig. 1 shows the XRD patterns of the $Ir/Ce_{0.75}Zr_{0.25}O_2$ catalyst. For the as-prepared catalyst, diffraction peaks assigned to cubic phase CeO_2 were observed (JCPDS 00-034-0394). Moreover, major diffraction angle (1 1 1) shifted from 28.5° to 28.9° compared to Ir/CeO_2 sample [32]. The other peaks also shifted to higher degree, probably due to the lattice shrinking of Ce^{4+} caused by the incorporation of Zr^{4+} which accounted for the evidence that the ionic radius of Zr^{4+} (0.083 nm) was lower than the value of Ce^{4+} (0.097 nm) [33]. It indicated the formation of CeO_2—ZrO_2 solid solution. The absence of Ir diffraction peaks suggested that a very small crystalline size of IrO_2 particle resulting from a strong interaction between IrO_2 and CeO_2—ZrO_2 support, was not detectable by X-ray technique. The average crystalline size of $Ce_{0.75}Zr_{0.25}O_2$ support was estimated to be about 7 nm. HRTEM

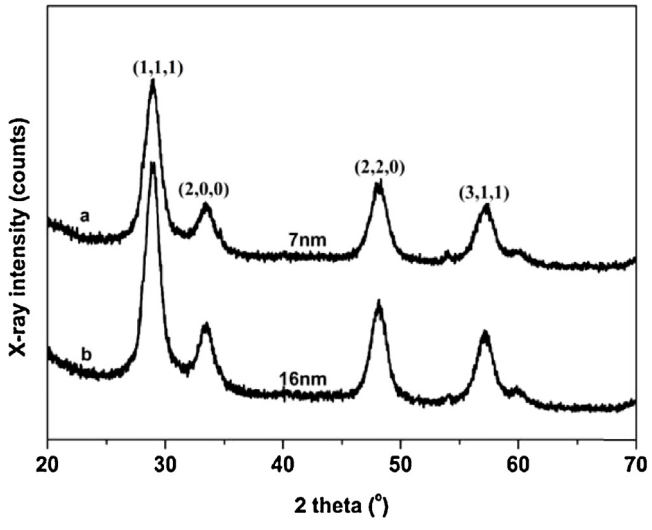


Fig. 1. XRD patterns of the $Ir/Ce_{0.75}Ze_{0.25}O_2$ catalysts. (a) fresh sample; (b) used catalyst at $C_3H_8/H_2O = 1/6$, $F_{react}/W_{cat} = 6000\ mL\ g_{cat}^{-1}\ h^{-1}$, 600 °C.

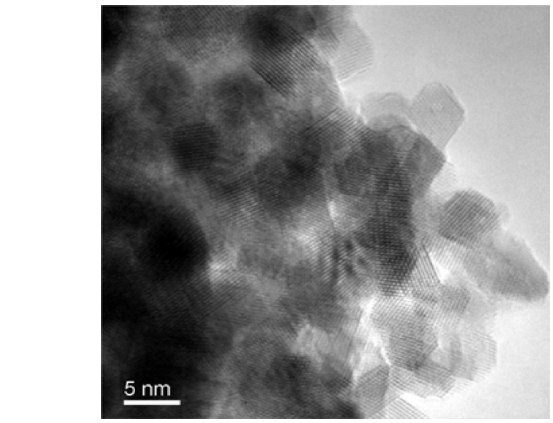


Fig. 2. HRTEM images of the as-prepared $Ir/Ce_{0.75}Zr_{0.25}O_2$ catalyst.

image of the as-prepared $Ir/Ce_{0.75}Zr_{0.25}O_2$ catalyst is shown in Fig. 2. The sizes of $Ce_{0.75}Zr_{0.25}O_2$ particles were in the range of 5–7 nm, in good agreement with XRD and BET measurements. Spherical support particles were poorly crystalline, and their composites were oriented randomly and interfaced epitaxially. Ir particles were difficult to see in line with XRD analysis probably due to the strong background influence of $Ce_{0.75}Zr_{0.25}O_2$ support or their small sizes.

OSC value of the $Ir/Ce_{0.75}Zr_{0.25}O_2$ catalyst indicated a strong interaction between Ir and support. Oxygen uptake was 292 μmolO_2/g for the pure support and 688 μmol O_2/g for the $Ir/Ce_{0.75}Zr_{0.25}O_2$ catalyst. In fact, $Ce_xZr_{1-x}O_2$ is known to possess an intrinsically high OSC, and the addition of noble metals could promote this property significantly [34,35]. This capacity is associated to the storage/release of oxygen via the Ce^{4+}/Ce^{3+} redox cycle. The particular role of the noble metal in OSC enhancement remains a matter of debate. One possible explanation was that part of the added noble metal formed small oxide clusters within the CeO_2 fluorite structure, acting as privileged pathway for oxygen storage and diffusion [36].

Fig. 3 compares the TPR profiles of the $Ir/Ce_{0.75}Zr_{0.25}O_2$ catalyst and the $Ce_{0.75}Zr_{0.25}O_2$ support. TPR profiles of pure $Ce_{0.75}Zr_{0.25}O_2$ support mainly exhibited two reduction peaks, appearing at 281 °C (H_2 consumption: 282 μmol/g) and 469 °C (H_2 consumption: 556 μmol/g), respectively. It was known that no obvious reduction of ZrO_2 was observed below 600 °C [37,38]. Hence, the above two peaks were assigned to the reduction of surface CeO_2. With

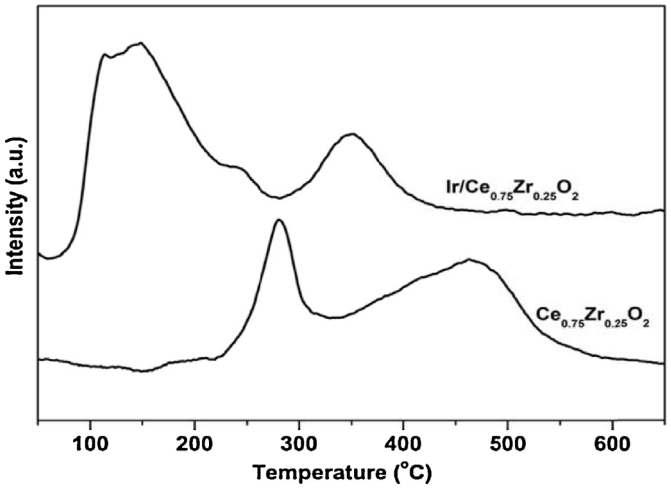


Fig. 3. TPR profiles of the $Ce_{0.75}Zr_{0.25}O_2$ and $Ir/Ce_{0.75}Zr_{0.25}O_2$ catalysts.

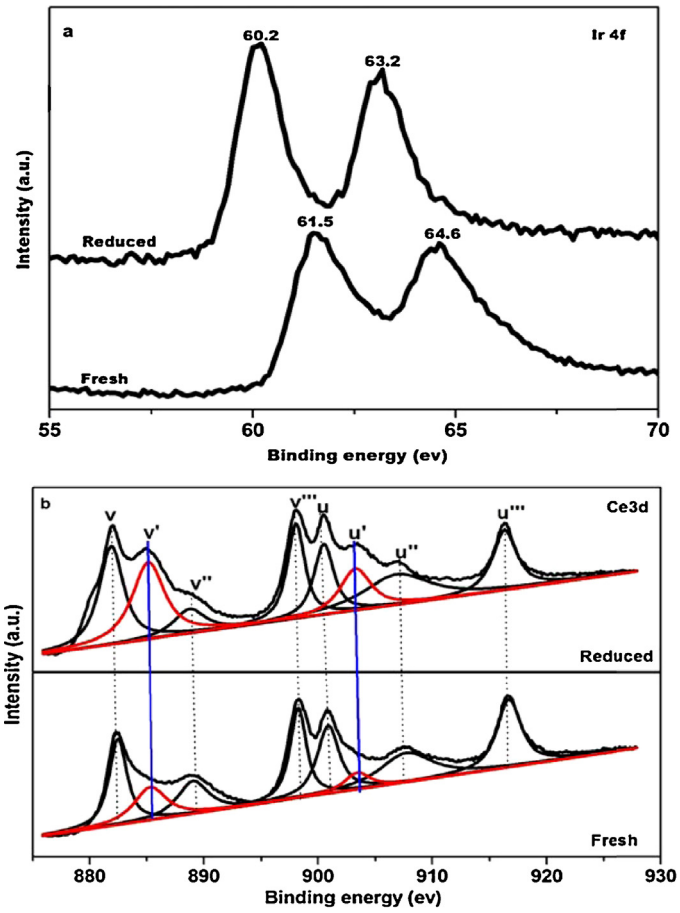


Fig. 4. XPS spectra of the $Ir/Ce_{0.75}Zr_{0.25}O_2$ catalyst. (a) Ir4f (b) Ce3d.

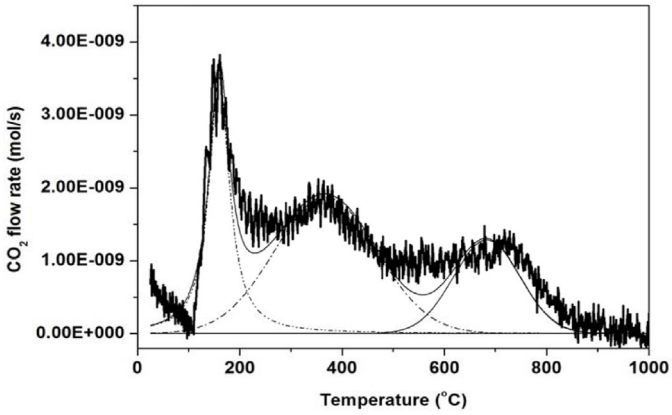


Fig. 5. CO_2—TPD pattern of the $Ir/Ce_{0.75}Zr_{0.25}O_2$ catalyst.

the addition of Ir, the reduction temperature of the mixed oxide shifted to the lower temperature region. The reduction peak at 132 °C was attributed to the combined reduction of Ir oxide and the partial surface CeO_2 because H_2 consumption (1147 μmol/g) was much larger than the amount of hydrogen required for the stoichiometric reduction of IrO_2 to Ir (211 μmol/g). Another peak at 350 °C (257 μmol/g) was also attributed to the reduction of surface CeO_2 that might be a little far from the active metal Ir. Hence, the presence of Ir greatly facilitated the reduction of CeO_2, indicating a strong interaction between Ir and CeO_2. The promotion of CeO_2 reduction by noble metal was due to the hydrogen spill-over phenomenon [28]. Indeed, it was supposed that hydrogen, once dissociated on metallic Ir, was able to spill over to the support and reduce it at lower temperatures. Evaluating the H_2 consumption, it indicated that $Ir/Ce_{0.75}Zr_{0.25}O_2$ (1393 μmol/g) was much higher than the value of Ir/CeO_2 catalyst (1195 μmol/g) [32]. This result was in good agreement with the previous findings [39], suggesting that the presence of ZrO_2 favored the reduction of CeO_2 due to the higher oxygen mobility in lattice and the creation of vacancies.

The chemical species presented on the catalyst surfaces were also evaluated by XPS technique. The energy regions of Ir4f, Ce3d core levels in oxidized and reduced samples were recorded. As shown in Fig. 4a. The Ir4f spectrum of the oxidized sample presented a doublet centered at around 61.7 eV and 64.7 eV, which corresponded to the binding energy of IrO_2 species. The spectra of the reduced sample exhibited a doublet centered at 60.6 eV and 63.6 eV, characteristic of the binding energy of metallic Ir. It indicated that most of the Ir oxide species were reduced to metallic Ir after reduction at 400 °C. As presented in Fig. 4b, the curves of Ce3d spectra were composed of eight peaks corresponding to four pairs of spin-orbit doublets. Letters u and v referred to the $3d_{3/2}$ and $3d_{5/2}$ spin-orbit components, respectively. The peaks marked as u, u" and u"' were assigned to $Ce^{4+}3d_{3/2}$, while the peaks labeled as v, v" and v"' were attributed to $Ce^{4+}3d_{5/2}$. The peaks of u' and v' were assigned to Ce^{3+} species [40]. The proportion of Ce^{3+} with respect of total cerium was calculated according to the procedure of [41]:

$$\text{Ce(III)}(\%) = \frac{100 \times [s(u') + s(v')]}{\Sigma[s(u) + s(v)]}$$

The relative concentration of Ce^{3+} species drastically increased from 15.9% (oxidized sample) to 28.2% (reduced sample). As reported in the literature [42], the presence of Ce^{3+} was associated with the formation of oxygen vacancies. More oxygen vacancies facilitated the water activation in hydrocarbon reforming. It also favored not only the diffusion of bulk oxygen to CeO_2 surface but also the surface transfer of OH groups and/or oxygen which was helpful for the coke removal.

The basicities of the samples were evaluated by means of CO_2—TPD. As shown in Fig. 5, three main CO_2 desorption peaks separately located at ca.160 °C(LT), 362 °C(MT) and 683 °C(HT) were observed in the CO_2—TPD profile of the $Ir/Ce_{0.75}Zr_{0.25}O_2$ sample [43]. These desorption zones were related to the strength of basic sites on which CO_2 was chemisorbed. The LT peak was attributed to the formation of hydrogencarbonates resulting from the interaction of CO_2 with weak basicity hydroxyl groups on the surface of the support. The MT peak corresponded to the formation of bridged and bidentate carbonates, and it was associated with the presence of $M^{x+}...O^{2-}$ pairs of intermediate basic strength. The HT peak could tentatively be assigned to the formation of relatively stable carbonates coming from the reaction of low coordination O^{2-} ions with CO_2 [44]. It was known that basic sites could efficiently inhibit carbon formation to guaranty the catalyst stability [45].From the above characterization results, one could conclude that Ir species were highly dispersed on the support surface and the redox capacity of $Ce_{0.75}Zr_{0.25}O_2$ support was greatly enhanced due to the strong interaction between Ir and support. In fact, the Ir-support interaction might accelerate the catalyst activity in propane steam reforming for hydrogen production.

Fig. 6 shows the distribution of the product concentrations calculated at equilibrium (by minimizing the free energy of formation) for further comparison with the experimental data. Propane is converted completely over the whole temperature range. Upon heating, hydrogen concentration increases and reaches a maximum at around 700 °C, simultaneously coinciding with the total disappearance of methane. CO_2 concentration also presents a maximum at ca. 580 °C and steadily declines at higher temperature. CO develops only at high temperature, as expected from the reverse water

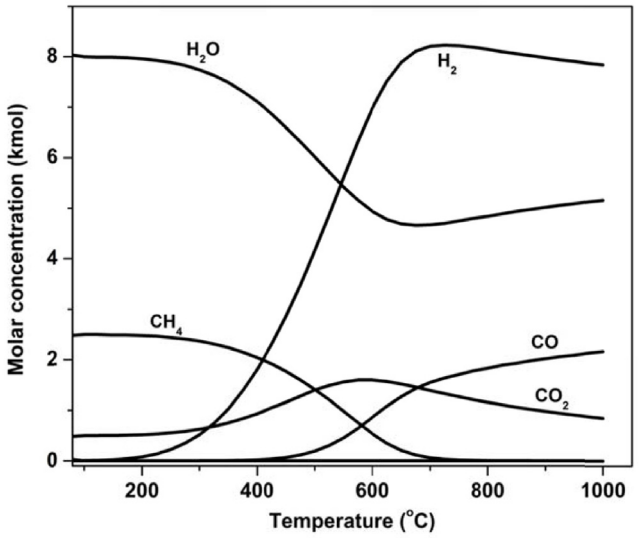


Fig. 6. Effect of reaction temperature on equilibrium concentrations for the propane steam reforming ($C_3H_8/H_2O = 1/6$, pressure: 1 atm).

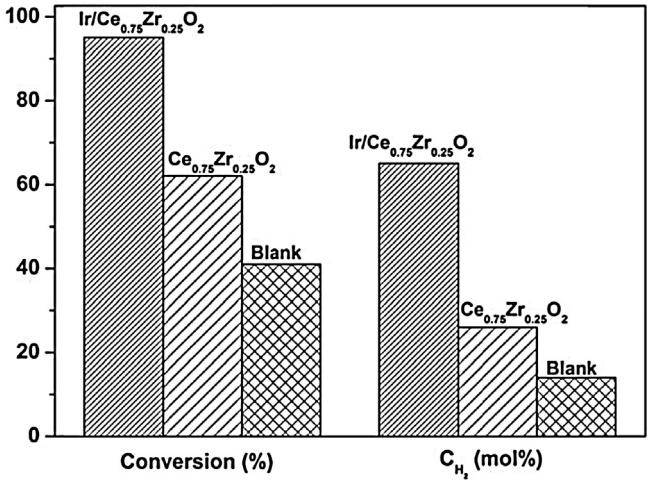


Fig. 8. Comparison of propane conversion and hydrogen concentration over $Ir/Ce_{0.75}Zr_{0.25}O_2$, $Ce_{0.75}Zr_{0.25}O_2$ and blank conditions. ($C_3H_8/H_2O = 1/6$, $F_{react}/W_{cat} = 6000\ mL\ g_{cat}^{-1}\ h^{-1}$ W_{cat}: catalyst weight, F_{react}: reactant flow rate; temperature: 600 °C).

gas shift reaction. No other C_3 or C_2 products are observed, being not stable enough thermodynamically.

Fig. 7 presents the evolution of the propane conversion and the product concentrations as a function of the reaction temperature for propane steam reforming over $Ir/Ce_{0.75}Zr_{0.25}O_2$ catalyst. It was obvious that both propane conversion and hydrogen concentration increased progressively with the temperature. At 700 °C, hydrogen concentration in the outlet gas could be achieved to about 76 mol%. Concerning the distribution of C-containing products, significant amount of CO_2 was formed at the lower temperature probably due to the water gas shift reaction. That was also why only trace amount of CO (2.5 mol%) was observed at 450 °C. However, with further heating, both rapid increase of CO concentration and gradual decrease in the CO_2 formation was observed indicating that the reverse water gas shift reaction, which was thermodynamically feasible, occurred. Upon heating, the amount of methane drastically declined due to methane steam reforming, as predicted by thermodynamics. At 700 °C, methane was almost completely reformed into hydrogen and CO. About 1–1.5 mol% C_3H_6 was observed over the entire temperature range probably coming from propane dehydration reaction.

In the present case, additional experiments have been carried out with $Ce_{0.75}Zr_{0.25}O_2$ support or under blank conditions in order to elucidate the reactions caused by the support and the contribution from gas-phase reactions. The results are shown in Fig. 8. C_3H_8 conversion drastically decreased with only $Ce_{0.75}Zr_{0.25}O_2$ support or under blank conditions. The related hydrogen concentration followed the similar trend remaining substantially lower than the value obtained over Ir catalyst. This indicated that: (i) surface reactions were in any case much faster and more selective than gas phase ones; (ii) heterogeneous reactions, taking place on Ir or Ir-support interfaces, are the main contribution to the formation of H_2 and propane conversion. In the previous studies of Shen group [19,21], active metal Ir exhibited excellent C—C bond dissociation capacity, which could enhance ethanol conversion. Hence, with the addition of Ir, it also could accelerate propane conversion to C_1 products and hydrogen.

In order to further investigate the improvement of Zr addition, the reforming process has also been studied over Ir/CeO_2, $Ir/Ce_{0.75}Zr_{0.25}O_2$, Ir/ZrO_2 catalysts. The results were presented in Fig. 9. Among the catalyst examined, Ir/ZrO_2 sample was the least active and selective. It was known that ZrO_2 support did not possess OSC like CeO_2 support which was crucial for the activation

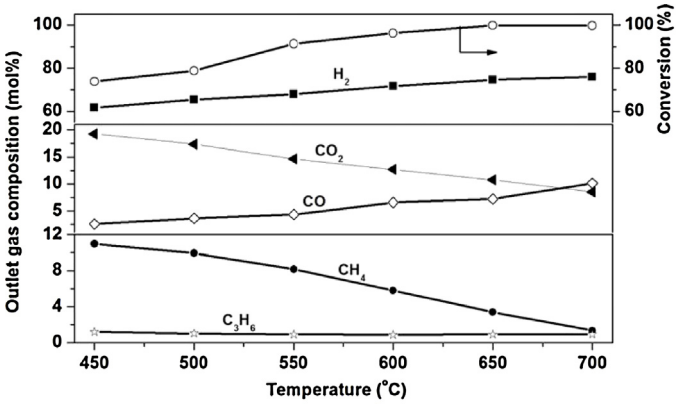


Fig. 7. Effect of reaction temperature on the product distributions for propane steam reforming. ($C_3H_8/H_2O = 1/6$, $F_{react}/W_{cat} = 6000\ mL\ g_{cat}^{-1}\ h^{-1}$ W_{cat}: catalyst weight, F_{react}: reactant flow rate).

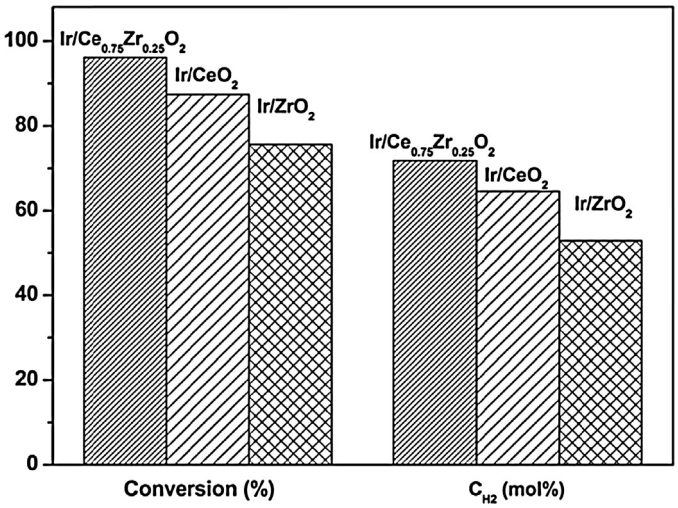


Fig. 9. Comparison of propane conversion and hydrogen concentration over Ir/CeO_2, $Ir/Ce_{0.75}Zr_{0.25}O_2$ and Ir/ZrO_2. ($C_3H_8/H_2O = 1/6$, $F_{react}/W_{cat} = 6000\ mL\ g_{cat}^{-1}\ h^{-1}$ W_{cat}: catalyst weight, F_{react}: reactant flow rate; temperature: 600 °C).

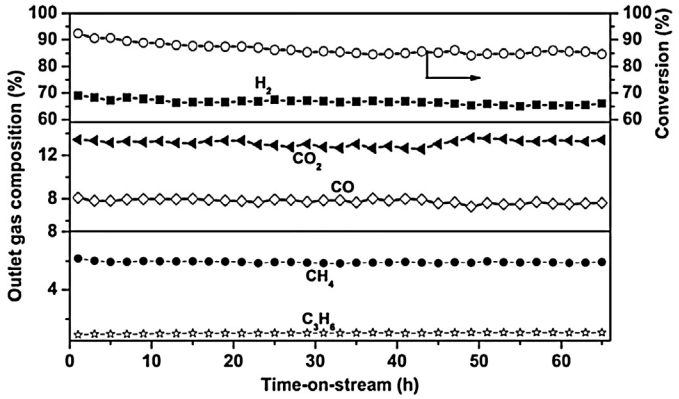


Fig. 10. Stability test for propane steam reforming at 600 °C. ($C_3H_8/H_2O = 1/6$, $F_{react}/W_{cat} = 6000\ mL\ g_{cat}^{-1}\ h^{-1}$ W_{cat}: catalyst weight, F_{react}: reactant flow rate).

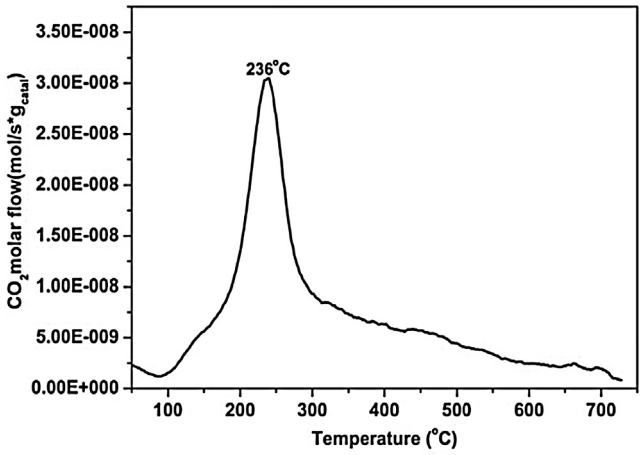


Fig. 12. Temperature-programmed oxidation of the used $Ir/Ce_{0.75}Zr_{0.25}O_2$ catalyst for propane steam reforming at 600 °C.

of H_2O and diffusion of intermediates to Ir-support surface [18]. $Ir/Ce_{0.75}Zr_{0.25}O_2$ catalyst exhibited the highest catalytic activity and hydrogen selectivity. It was probably assigned to its higher OSC, oxygen mobility and support defects after the addition of Zr into CeO_2 support.

The development of stable catalyst is one of the most important issues in hydrogen production from propane, particularly with stoichiometric feed compositions where no excess water is available to remove carbon deposits that are detrimental to the catalyst stability. Long-term stability test of propane steam reforming over $Ir/Ce_{0.75}Zr_{0.25}O_2$ catalyst was conducted. As predicted in Fig. 10, propane conversion decreased from about 95% to 87% during the initial period of 10–12 h on stream, then both propane conversion and product concentrations almost kept constant over the all remaining testing period. The concentrations of H_2, CO, CO_2 and CH_4 in the outlet stream were about 67 mol%, 9 mol%, 14 mol% and 8 mol%, respectively.

In order to further elucidate the excellent stability of the investigated system, several characterizations (XRD, HRTEM, TPO) were done on the aged catalysts. Fig. 1(b) shows the XRD patterns of the used $Ir/Ce_{0.75}Zr_{0.25}O_2$ catalyst. No diffraction reflexes of Ir species were observed as before testing, providing evidence that no aggregation or sintering of Ir particles occurred during the stability tests. The particle size of CeO_2 increased to about 16 nm during the course of reaction. The small CeO_2 nanoparticles with high surface energy in the fresh catalyst tended to aggregate into larger particles under the reaction conditions, similar to a hydrothermal process.

Fig. 11 presents the HRTEM images of the used catalyst. Along with the increase in particle size, the morphology of the support particles also shifted from spherical in the as-prepared sample to polygonal crystallite cubes after the tests. As for Ir species, they could be observed on the aged samples (at variance with the fresh one) because CeO_2 particles were sintered enough to allow us to differentiate Ir from Ce aggregates. The observed Ir particles presented a mean size in the 2–3 nm range indicating that they were still highly dispersed on the support surface, maintaining sufficient Ir-support interfacial areas where the reaction occurred. No serious sintering of Ir species was observed after stability test. This demonstrated that the strong Ir-support interaction efficiently prevented sintering of the Ir particles during the long-term test. No obviously carbonaceous deposits were observed in the HRTEM images indicating that the equilibrium between the coke deposition and its gasification during the reaction has been established. Mattos et al. [46] considered that the high amount of CeO_2 support oxygen vacancies near the metal particles promoted the carbon removal from the metallic surface, which took place at the metal-support interfacial perimeter.

TPO experiment was also performed in order to detect eventual carbonaceous formation over the aged catalyst. Fig. 12 shows the TPO profile of the used catalyst for propane steam reforming at 600 °C. It was apparent that CO_2 was produced mainly at about 236 °C by the oxidation of easy oxidized carbon deposits. The observation of small shoulder at higher temperature might be related to the more stable carbon deposits such as C_3H_6 which would be precursor of stable polymeric coke. However, the total amount of carbon was almost negligible (0.31 $mgC/g_{cat}/h$).

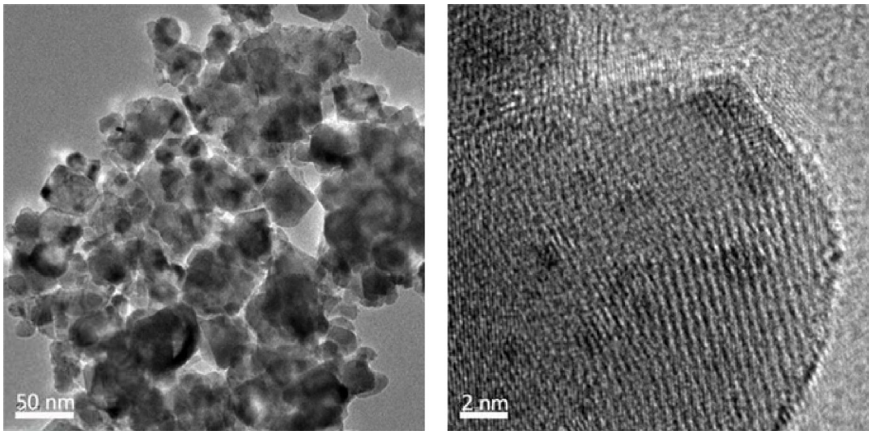


Fig. 11. HRTEM images of the aged $Ir/Ce_{0.75}Zr_{0.25}O_2$ catalyst for propane steam reforming.

Based on the above results, it is elucidated that the strong Ir-support interaction efficiently prevents active metal Ir sintering and coke formation, thus guaranteeing the catalyst stability.

4. Conclusion

$Ir/Ce_{0.75}Zr_{0.25}O_2$ catalyst was shown to be highly active and stable for propane steam reforming, even with a stoichiometric feed composition at 600 °C for 65 h on stream. There was no obvious deactivation with a constant effluent gas composition. The doping of ZrO_2 into the CeO_2 lattice greatly improved the redox property of the CeO_2 by creating more surface oxygen vacancies. Structural analysis of the aged catalysts indicated that the 2–3 nm Ir particles remained highly dispersed on the enlarged support particles. $Ce_{0.75}Zr_{0.25}O_2$ support probably prevented the highly dispersed Ir particles from sintering and effectively inhibited coke deposition through the strong Ir-support interaction.

Acknowledgements

We gratefully acknowledge the financial support from Program for Liaoning Excellent Talents in University (Grant no. LJQ2014053); Key Laboratory of Renewable Energy and Gas Hydrate, Chinese Academy of Sciences (Grant no. y407k21001) and National Natural Science Foundation of China (Grant no. 21303185).

References

[1] L.V. Mattos, G. Jacobs, B.H. Davis, F.B. Noronha, Chem. Rev. 112 (2012) 4094–4123.
[2] H.L. Chen, H.M. Lee, S.H. Chen, Y. Chao, M.B. Chang, Appl. Catal. B 85 (2008) 1–9.
[3] G.W. Wu, S.R. Li, C.X. Zhang, T. Wang, J.L. Gong, Appl. Catal. B 144 (2014) 277–285.
[4] O. Mihai, A. Fathali, X. Auvray, L. Olsson, Appl. Catal. B 160–161 (2014) 480–491.
[5] Z.O. Malaibari, A. Amin, E. Croiset, W. Epling, Int. J. Hydrogen Energy 39 (2014) 10061–10073.
[6] Y.J. Bang, S.J. Han, J. Yoo, J.H. Choi, J.K. Lee, J.H. Song, J.W. Lee, I.K. Song, Appl. Catal. B 148–149 (2014) 269–280.
[7] C. Agrafiotis, M. Roeb, C. Sattler, Renewable Sustainable Energy Rev. 42 (2015) 254–285.
[8] P.J. Woolcock, R.C. Brown, Biomass Bioenergy 52 (2013) 54–84.
[9] K. Lee, E. Lee, C.S. Song, M.J. Janik, J. Catal. 309 (2014) 248–259.
[10] R. Zapf, R. Thiele, M. Wichert, M. Oconnell, A. Ziogas, G. Kol, Catal. Commun. 41 (2013) 140–145.
[11] W.L.S. Faria, C.A.C. Perez, D.V. César, L.C. Dieguez, M. Schmal, Appl. Catal. B 92 (2009) 217–224.
[12] C.F. Wu, L.Z. Wang, P.T. Williams, J. Shi, J. Huang, Appl. Catal. B 108–109 (2011) 6–13.
[13] W.H. Fang, S. Paul, M. Capron, F. Dumeignil, L. Jalowiecki-Duhamel, Appl. Catal. B 152–153 (2014) 370–382.
[14] S.F. Weng, Y.H. Wang, C.S. Lee, Appl. Catal. B 134–135 (2013) 359–366.
[15] C. Resini, M.C.H. Delgado, L. Arrighi, L.J. Alemany, R. Marazza, G. Busca, Catal. Commun. 6 (2005) 441–445.
[16] H.J. Lee, Y.S. Lim, N.C. Park, Y.C. Kim, Chem. Eng. J. 146 (2009) 295–301.
[17] M. Chrisian, Mitchell J.A. Kenis, Lab Chip 6 (2006) 1328–1337.
[18] W.J. Cai, F.G. Wang, C. Daniel, A.C. van Veen, Y. Schuurman, C. Descorme, H. Provendier, W.J. Shen, C. Mirodatos, J. Catal. 286 (2012) 137–152.
[19] W.J. Cai, F.G. Wang, E.S. Zhan, A.C. van Veen, C. Mirodatos, W.J. Shen, J. Catal. 257 (2008) 96–107.
[20] W.J. Cai, F.G. Wang, A.C. van Veen, C. Descorme, Y. Schuurman, C. Mirodatos, W.J. Shen, Int. J. Hydrogen Energy 35 (2010) 1152–1159.
[21] W.J. Cai, B.C. Zhang, Y. Li, Y.D. Xu, W.J. Shen, Catal. Commun. 8 (2007) 1588–1594.
[22] W.J. Cai, P. Ramirez de la Piscina, N. Homs, Appl. Catal. B 145 (2014) 56–62.
[23] W.J. Cai, N. Homs, P. Ramirez de la Piscina, Green Chem. 14 (2012) 1035–1043.
[24] R. Trane-Restrup, S. Dahl, A.D. Jensen, Int. J. Hydrogen Energy 38 (2013) 15105–15118.
[25] M. Taillades-Jacquin, C. Resini, K.E. Liew, G. Taillades, I. Gabellini, D. Wails, J. Roziere, D. Jones, Appl. Catal. B 142–143 (2013) 112–118.
[26] W.J. Cai, N. Homs, P. Ramirez de la Piscina, Appl. Catal. B 150–151 (2014) 47–56.
[27] S. Abdollahzadeh-Ghom, C. Zamania, T. Andreub, M. Epifanic, J.R. Morantea, Appl. Catal. B 108–109 (2011) 32–38.
[28] G. Balducci, J. Kašpar, P. Fornasiero, M. Graziani, M.S. Islam, J.D. Gale, J. Phys. Chem. B 101 (1997) 1750–1753.
[29] P. Biswas, D. Kunzru, Int. J. Hydrogen Energy 32 (2007) 969–980.
[30] H.S. Roh, A. Platon, Y. Wang, D.L. King, Catal. Lett. 110 (2006) 1–5.
[31] B.D. Cullity, Elements of X-ray Diffraction, second ed., Addison-Wesley, Menlo Park, CA, 1978, pp. 102.
[32] W.J. Cai, B.C. Zhang, Y. Li, Y.D. Xu, W.J. Shen, Catal. Commun. 8 (2007) 1588–1594.
[33] L. Pino, A. Vita, F. Cipiti, M. Lagana, V. Recupero, Appl. Catal. A 306 (2006) 68–77.
[34] M. Li, Z.G. Liu, Y.H. Hu, M.T. Wang, H.Q. Li, J. Rare Earth 26 (2008) 357–361.
[35] J. Mikuloá, J. Barbier Jr., S. Rossignol, D. Mesnard, D. Duprez, C. Kappenstein, J. Catal. 251 (2007) 172–181.
[36] E.M. Sadovskaya, Y.A. Ivanova, L.G. Pinaeva, G. Grasso, T.G. Kuznetsova, A.C. van Veen, V.A. Sadykov, C. Mirodatos, J. Phys. Chem. A 111 (2007) 4498–4505.
[37] S.K. Maity, M.S. Rana, B.N. Srinivas, S.K. Bej, T.S.R. Prasado Rao, J. Mol. Catal. A 153 (2000) 121–127.
[38] X.F. Dong, H.B. Zou, W.M. Lin, Int. J. Hydrogen Energy 31 (2006) 2337–2344.
[39] P.P. Silva, F.A. Silva, L.S. Portela, L.V. Mattos, F.B. Noronha, C.E. Hori, Catal. Today 107–108 (2005) 734–740.
[40] J. Fan, X.D. Wu, Q. Liang, R. Ran, D. Weng, Appl. Catal. B 81 (2008) 38–48.
[41] B. Zhang, G.F. Li, C.H. Ge, Q.Y. Wang, R.X. Zhou, Appl. Catal. B 96 (2010) 338–349.
[42] C. Bozo, N. Guilhaumw, J.M. Herrmann, J. Catal. 203 (2001) 393–406.
[43] W. Khaodee, B. Jongsomjit, S. Assabumrungrat, P. Praserthdam, S. Goto, Catal. Commun. 8 (2007) 548–556.
[44] S. Sato, R. Takahashi, M. Kobune, H. Gotoh, Appl. Catal. A 356 (2009) 57–63.
[45] H.S. Roh, K.W. Jun, W.S. Dong, J.S. Chang, S.E. Park, Y. Joe, J. Mol. Catal. A 181 (2002) 137–142.
[46] L.V. Mattos, F.B. Noronha, J. Catal. 233 (2005) 453–463.